Ceramics International xxx (xxxx) xxx

Contents lists available at ScienceDirect

Ceramics International

journal homepage: www.elsevier.com/locate/ceramint

Antibacterial effect and cell metabolic activity of $Na_2CaSi_2O_6$, β-$NaCaPO_4$, and β-$NaCaPO_4$-SiO_2 *versus* hydroxyapatite

R.L. Siqueira [a,*], N. Maurmann [b], P.K.P. Gaio [b,c], D.P. Pereira [b,c], P. Pranke [b,d], L.T.A. Cintra [e], C.H.G. Martins [f], O. Peitl [a], E.D. Zanotto [a]

[a] *Laboratório de Materiais Vítreos, Departamento de Engenharia de Materiais, Universidade Federal de São Carlos, 13565-905, São Carlos, SP, Brazil*
[b] *Laboratório de Hematologia e Células-tronco, Faculdade de Farmácia, Universidade Federal Do Rio Grande Do Sul, 90610-000, Porto Alegre, RS, Brazil*
[c] *Universidade Federal de Ciências da Saúde de Porto Alegre, 90050-170, Porto Alegre, RS, Brazil*
[d] *Instituto de Pesquisa Com Células-tronco, 90020-010, Porto Alegre, RS, Brazil*
[e] *Faculdade de Odontologia de Araçatuba, Departamento de Odontologia Preventiva e Restauradora, Universidade Estadual Paulista Júlio de Mesquita Filho, 16015-050, Araçatuba, SP, Brazil*
[f] *Laboratório de Ensaios Antimicrobianos, Instituto de Ciências Biomédicas, Universidade Federal de Uberlândia, 38400-902, Uberlândia, MG, Brazil*

ARTICLE INFO

Handling Editor: Dr P. Vincenzini

Keywords:
Hydroxyapatite
45S5 bioglass
Combeite
Beta-rhenanite
Antibacterial activity
Cell viability

ABSTRACT

Hydroxyapatite ($Ca_5(PO_2)_3(OH)$) is extensively used in diverse clinical applications because of its relatively simple synthesis protocol, low cost, and chemical similarity to the mineral component of bones and teeth. Some limitations regarding bioactivity and antibacterial activity have motivated changes in its structure and the development of alternative materials to achieve better performances as bioceramics. In this study, the antibacterial effect and cell metabolic activity of the main crystalline phases ($Na_2CaSi_2O_6$, β-$NaCaPO_4$, and β-$NaCaPO_4$−SiO_2) derived from the original 45S5 bioactive glass were evaluated and compared with those induced by a commercial powder of hydroxyapatite. Powder samples of $Na_2CaSi_2O_6$, β-$NaCaPO_4$, and β-$NaCaPO_4$−SiO_2 were synthesized by a simple and reproducible solid-state reaction method. The β-$NaCaPO_4$−SiO_2 sample exhibited the strongest effect against *Pseudomonas aeruginosa*, *Staphylococcus aureus*, and *S. epidermidis*, which are bacteria that normally colonize the skin but can become opportunistic pathogens when the host's resistance is low. All bacteria were eliminated within 5 min in the direct-contact test, an effect that is likely associated with changes in pH in the microenvironment generated from the partial solubilization of the material and the action of certain released ions, such as Ca^{2+}. In *vitro* experiments with human cells, no sample showed cytotoxicity, and the β-$NaCaPO_4$−SiO_2 sample stood out once more inducing the most positive effect on keratinocyte and stem cell viability. Overall, the tested materials demonstrated similar or better (β-$NaCaPO_4$−SiO_2) biochemical properties than hydroxyapatite. This finding encourages us, and perhaps other research groups, to assess the bioperformance of these materials more comprehensively, aiming at the development of new products for use in tissue engineering.

1. Introduction

Ceramic materials based on hydroxyapatite ($Ca_5(PO_2)_3(OH)$) are useful in various medical applications, including implants for bone repair and reconstruction, tissue engineering, controlled drug delivery, cancer therapies, and as a fluorescent bioimaging agent [1]. The great interest in using hydroxyapatite as a bioceramic lies in its high chemical and crystallographic semblance to the mineral component of bones and teeth. In addition, hydroxyapatite has some advantages over other bioceramics, such as intrinsic biocompatibility and bioactivity, relatively simple synthesis protocols (including the preparation of nanoparticles with specific sizes and shapes), facile functionalization and surface modification, and capacity to be loaded with a wide range of therapeutic agents [1–3].

Although hydroxyapatite presents several benefits, some shortcomings regarding antibacterial activity and bioactivity need to be overcome to direct its use toward more specific medical applications. Hydroxyapatite doped with different foreign ions has been intensely researched to improve these issues, as well as its association with bioactive glass particles to formulate composites [3]. Bioactive glasses are materials

* Corresponding author.
E-mail address: rastosfix@gmail.com (R.L. Siqueira).

https://doi.org/10.1016/j.ceramint.2023.06.256
Received 7 February 2023; Received in revised form 22 June 2023; Accepted 26 June 2023
Available online 28 June 2023

that interact much quicker and positively with hard and soft tissues [3,4] and, currently, there are many compositions designed for more specific applications [5]. The first and most tested bioactive glass is a silicate with composition $45SiO_2-24.5CaO-24.5Na_2O-6P_2O_5$ (wt%) developed in the late 1960s and known worldwide by its trademark Bioglass® [6]. It is also called 45S5 bioactive glass or 45S5 bioglass — common terms referring to its original composition.

Unlike crystalline materials such as hydroxyapatite, bioactive glasses do not show long-range order and significant symmetry in their atomic arrangement, but they can be crystallized (re-ordered) in a controlled manner by different processing methods involving heat treatments [7]. Thus, through the controlled crystallization of glasses, it is possible to obtain glass-ceramics containing at least one type of functional crystalline phase and a residual glass — substantially improving the performance of their mechanical and other properties. In this case, the material biological interactivity becomes dependent on the crystal phases formed and the residual glass fraction because of their intrinsic degradation rates and the ions (type and amount) that are released at the implant site. Consequently, for some compositions, the crystallization process may reduce the material interactivity but not necessarily do so, still being possible to obtain polycrystalline materials with performance comparable to that of Bioglass®, a material tested in numerous human clinical trials [8]. For example, regarding antibacterial activity, one of the aspects covered in this study, the $Na_2CaSi_2O_6$ phase exhibits this property against some bacteria of the oral cavity intrinsically [9,10], similarly to the 45S5 bioactive glass. The antibacterial activity of these materials and other bioceramics is normally attributed to the alkaline microenvironment generated from their degradation and the action of certain ions that are released in the process, and these parameters are directly related to the structure and composition of the materials [9–11]. The observed effect is dose-dependent, hence, based on this principle, any material can be tested for this purpose, including glasses, glass-ceramics, and ceramics, such as the crystalline samples evaluated in this study. Material performance can be improved by incorporation elements with a broad spectrum of antibacterial action, such as Ag, Cu, Ga, Zn, Mo — also improving and/or causing stimulating effects on osteogenesis and angiogenesis [1–3,5,10–12].

In one of the first studies addressing the crystallization of bioactive glasses, with compositions similar to that of the 45S5 bioactive glass to produce glass-ceramics [13], the main crystalline phase formed was attributed to combeite ($Na_2Ca_2Si_3O_9$). The formation of a secondary apatitic phase (not yet indexed) was also observed in that study with additional thermal treatments performed to check the phosphorus stability in the glass system. A few years later, other researchers [14] indicated the formation of a combeite-like phase, $Na_2CaSi_2O_6$, rather than the classical $Na_2Ca_2Si_3O_9$ phase in an almost fully crystallized 45S5-based glass, and this result was later reinforced by Lefebvre and coauthors [15]. Both ($Na_2Ca_2Si_3O_9$ and $Na_2CaSi_2O_6$) phases are commonly associated with the crystallization of 45S5 bioactive glass because they present similar X-ray diffraction patterns since the combeite phase can form a continuous solid-solution series ($Na_{3-x}Ca_{1.5+0.5x}Si_3O_9$ ($0 \leq x \leq 1$)), as suggested by Moir and Glasser [16]. Lefebvre and coauthors also detected the formation of a secondary phosphate phase in the system and attributed it to the silicorhenanite ($Na_2Ca_4(PO_4)_2SiO_4$) phase. Beta-rhenanite (β-$NaCaPO_4$) is another phase normally attributed to the phosphate formed in bioceramics with compositions of the SiO_2–CaO–Na_2O–P_2O_5 system [17–21]. This is not a simple matter as the phosphorus content in these bioceramics is usually equal to or less than that in the 45S5 bioactive glass composition (6 wt% or 2.6 mol%), forming only a small fraction of phosphate and thus rendering the phase indexation difficult. Moreover, $Na_2Ca_4(PO_4)_2SiO_4$ and β-$NaCaPO_4$ show very similar X-ray diffraction patterns. These phases are also formed under milder temperatures employing the sol-gel process [22–27]; however, none of these studies have discussed these phases singly or evaluated their capacity to induce cell viability and antibacterial activity.

Hence, based on these observations, in this study, powder samples of $Na_2CaSi_2O_6$, β-$NaCaPO_4$, and $Na_2Ca_4(PO_4)_2SiO_4$ were synthesized to evaluate their antibacterial effect against some microorganisms and the keratinocyte and human stem cell metabolic activities in comparison with those of a commercial powder of hydroxyapatite, which is a phosphate phase recognized and extensively used in various medical applications [1–3]. Since hydroxyapatite has some intrinsic limitations, such as its antibacterial activity, our aim was to verify the potential of these crystalline materials derived from the 45S5 bioactive glass composition in a comparative way and, consequently, perhaps provide an evolution in this field by assessing some of their biological properties that have not yet been investigated.

2. Materials and methods

2.1. Synthesis of the powders

For the synthesis procedures, silicon dioxide (SiO_2 99.9%), calcium ($CaCO_3$ 99.5%) and sodium (Na_2CO_3 99.5%) carbonates, and calcium hydrogen phosphate ($CaHPO_4$ 99.0%) were used to achieve the nominal compositions of the $Na_2CaSi_2O_6$, β-$NaCaPO_4$, and modified β-$NaCaPO_4$ containing 12.30 wt% SiO_2 to reach the silicorhenanite stoichiometry ($Na_2Ca_4(PO_4)_2SiO_4$). Commercial powder of hydroxyapatite (≥97%) provided by Sigma-Aldrich, the same supplier of the other aforementioned chemicals, was used for comparative purposes.

To synthesize 100 g of each sample, the relative proportions of each chemical in the batch were calculated using the freely available GlassPanacea® software [28,29], which made this step fast and accurate. After weighing and mixing the chemicals in a polyethylene bottle, each mixture was homogenized in a laboratory jar mill (Solab SL-34) for 12 h and then thermally treated at approximately 1000 °C for 500 min in an electric furnace, following the protocol developed in a previous study [10,20], involving an easy-to-implement solid-state reaction method to prepare bioactive ceramics in different forms. After completing the thermal treatments, the samples were cooled naturally and desegregated manually in an agate mortar. Finally, the powders with particles <50 μm were selected for characterization.

2.1.1. Characterization

To analyze the crystalline phases formed in the particulate materials, X-ray diffraction (XRD) was performed on a Shimadzu LabX XRD-6000 diffractometer operating with CuKα radiation ($\lambda = 0.15418$ nm). The diffraction patterns were obtained for 2θ ranging from 10 to 70° in a continuous scan mode at 0.5°/min. To assist in structural characterization, samples of β-$NaCaPO_4$ and β-$NaCaPO_4$–SiO_2 were also analyzed by Fourier Transform Infrared (FTIR) spectroscopy on a Shimadzu IRPrestige-21 spectrometer equipped with an attenuated total reflectance (ATR) module. All spectra were collected with at least 50 scans with a spectral resolution of 4 cm^{-1} from 1400 to 400 cm^{-1}.

The specific surface areas of the samples were determined by the Brunauer-Emmett-Teller (BET) method [30] using a Micromeritics ASAP 2020 analyzer by measuring nitrogen adsorption isotherms at 77 K. To remove any moisture, all samples were degassed at 200 °C for 720 min before analysis. Finally, the chemical composition of the powders was determined by X-ray fluorescence (XRF) spectrometry on a Philips PW2404 sequential XRF spectrometer.

2.2. Evaluation of antibacterial activity

The standard strains from the American Type Culture Collection (ATCC) selected for the test were the Gram-negative *P. aeruginosa* (ATCC 27853), and both Gram-positive *S. aureus* (ATCC 25923) and *S. epidermidis* (ATCC 12228). The Brain Heart Infusion broth (BHIb) and agar (BHIa) pair (Difco™), supplemented with 5% defibrinated sheep blood, was used as culture medium. To evaluate the antibacterial activity, two methods were used similar to a previous study [9,10], as

described below. At least three independent experiments were conducted for each sample, and all the results are expressed as mean values.

2.2.1. Agar dilution method

For the agar dilution method [31], all samples were sterilized at 200 °C for 120 min and diluted in test tubes so that when 18 mL of BHIa were added to 2 mL of culture medium, the final concentrations reached 0.5, 1, 2, 4, 8, 16, and 24 mg/mL. The mixtures containing samples extracts were then homogenized and poured into Petri dishes (15 mm × 90 mm). Only BHIb, free of antimicrobial agent, and tetracycline (Sigma-Aldrich) with concentrations ranging from 2×10^{-3} to 2×10^{-5} mg/mL were used as the negative and positive control, respectively.

After incubation at 36 °C for 1440 min, bacterial suspensions from the fresh cultures of each bacterium were prepared in broth and standardized with turbidity corresponding to 0.5 on the McFarland scale (1.5×10^8 CFU/mL). The standardized suspensions were placed into a multiple inoculator and transferred to Petri dishes labeled based on the positive control, from the highest to the lowest dilution, ending on the negative control. When the inoculants were dry, the BHIa plates were incubated for another 1440 min and the minimum inhibitory concentration (MIC) values were determined as the lowest concentration of material capable of inhibiting the visible growth of bacterial colonies in the culture medium.

2.2.2. Direct contact method

Fresh cultures with bacteria incubated in BHIb for 24 h were centrifuged at 4000 RPM for 5 min and washed with a sodium chloride solution (0.9% NaCl). After that, a volume of solution was added to the sediments to reach a turbidity corresponding to ~3.0×10^6 CFU/mL. From each suspension, 10 μL were seeded onto the surface of the agar plates for a new incubation period and subsequent counting of colony-forming units per milliliter.

To test the samples with the direct contact method [32], 50 mg of each of them (after sterilization) were placed in four microtubes containing 30 μL of the bacterial suspension and homogenized on a shaker with addition of 470 μL of 0.9% NaCl solution. After 1 min, 20 μL aliquots were removed from one tube and seeded on the surface of the plate with agar for incubation and further reading of the bacterial growth. The same procedure was performed after 5, 10, and 60 min with the other tubes, respectively, to evaluate possible viable cells as a function of the contact time of the samples with the bacteria. The BHIb adequacy for bacterium growth was used as a reference for inoculum control. To verify the influence of pH variation in the medium caused by the samples, the same condition of the assay was reproduced, and the pH value was checked using a pH meter (Mettler Toledo S400-Bio) at each time. In a simplified way, $[H^+]$ and $[OH^-]$ can be related by the equilibrium constant ($K_w = 1 \times 10^{-14}$ at 25 °C) of water molecules ($H_2O \rightleftharpoons H^+ + OH^-$) [33]; thus, any decrease in $[H^+]$ is accompanied by an increase in $[OH^-]$ and vice versa. As the pH for an aqueous solution can be calculated using the relationship pH = - log $[H^+]$, the molar concentration of OH^- can be archived by $[OH^-] = 1 \times 10^{-14}/[H^+]$. This correlation was used to facilitate the identification and highlight the increase in pH in each sample during the test.

2.3. Culture conditions and tests with stem cell and keratinocyte

In the assay involving stem cells, fresh human dental pulp was harvested from deciduous teeth in resorption — approved by the Brazilian National Research Ethics Committee, Protocol CAAE number 36403514.6.0000.5347 — and the stem cells were extracted and isolated as previously described [34]. They were characterized as mesenchymal stem cell by morphological analysis of the cell cultures, *in vitro* differentiation, and immunophenotypic profile by flow cytometry [34,35] before being used in the experiments between the 4th and 8th passages. The stem cells were maintained in Dulbecco's Modified Eagle medium (DMEM, Sigma-Aldrich) with low glucose at pH adjusted to 7.2, supplemented with 2.5 g/L 4-(2-hydroxyethyl)-1-piperazineethanesulfonic acid (HEPES, Sigma-Aldrich), 3.7 g/L sodium bicarbonate (Neon), 10% heat-inactivated fetal bovine serum (Laborclin), 100 U/mL penicillin, and 0.1 mg/mL streptomycin (Sigma-Aldrich). This culture medium was used as a control in the experiments. For the other assay, immortalized human keratinocyte (HaCaT) cells were cultivated in DMEM high glucose at pH 7.2 and supplemented as previously described for stem cells.

The cell cultures were maintained at 37 °C in a humidified atmosphere with 5% CO_2. After reaching confluence, the cells were washed with phosphate buffer solution (PBS, Sigma-Aldrich) and then detached using a trypsin-EDTA solution (Sigma-Aldrich) diluted in PBS. Subsequently, the cells were centrifuged at 500 RCF for 5 min and seeded at 5 x 10^3 cell/cm^2 with fresh culture medium in cell culture flasks. As in the antibacterial activity assays, at least three independent experiments were performed for each sample and the results are expressed as mean values.

2.3.1. Mitochondrial activity test

Before testing, all samples were subjected to 1 h of UV light for sterilization. After that, each sample was mixed with DMEM low glucose supplemented until the final concentrations reached 0.5, 1.0, and 1.5 mg/mL. The characterized stem cells and keratinocytes were then seeded in 96-well culture plates at a density of 5×10^3 cells per well in 0.1 mL of culture medium. After 24 h, they were treated directly with 0.2 mL of each particulate sample suspended in the culture medium and cell viability was verified by the 3-(4,5-dimethylthiazol-2-yl)-2,5-diphenyltetrazolium bromide (MTT, Sigma-Aldrich) reduction method [35–37] after one day of treatment. The cells cultivated with DMEM low glucose supplemented without any sample were used as control. For cell viability measurement, the cells were incubated with 0.2 mL of 0.25 mg/mL MTT and 3 h later, the supernatant was carefully removed and 0.25 mL dimethyl sulfoxide (DMSO, Nuclear) were added to each well to dissolve the formed purple formazan dye in the living cells. Subsequently, 0.2 mL of the colored solution formed in each well were analyzed using a Multiskan™ FC Microplate Photometer (Thermo Fisher Scientific®) to measure its absorbance. Thus, cell viability was determined by absorbance in the range of 570–630 nm, considering the absorbance label subtraction concerning the control with untreated cells. Additionally, the influence of pH increase on the culture medium condition was verified with the MTT assay by comparing the control group with the stem cells cultivated in a culture medium added to 0.46 M NaOH.

2.4. Statistical analysis

Results of the biological tests were treated statistically using the one-way ANOVA followed by the Tukey's range test, and the results of cell viability determined from the control (untreated cells) were expressed as mean ± standard deviation (SD). Statistical differences were established at $p < 0.05$ using the freely available BioEstat software.

3. Results and discussion

3.1. Characterization of the powders

The BET surface area of the $Na_2CaSi_2O_6$, β-$NaCaPO_4$, and β-$NaCaPO_4$−SiO_2 powders were 0.89, 0.93, and 0.88 m^2/g, respectively. These low surface area values are typical of materials subjected to thermal treatments or synthesized at high temperatures for relatively long times, as in the solid-state reaction method employed in this study. The commercial $Ca_5(PO_4)_3OH$ exhibited a BET surface area of 7.8 m^2/g. As discussed later, this ~10x larger surface of hydroxyapatite did not contribute to its performance in the current tests. The chemical compositions of all samples are given in Table 1, showing a good agreement with the expected stoichiometry of each desired phase. This result

Table 1
Quantitative XRF chemical analysis of the synthesized materials (normalized to 100%).

Component (wt%)	nominal	$Na_2CaSi_2O_6$	nominal	β-$NaCaPO_4$	nominal	β-$NaCaPO_4$−SiO_2
% SiO_2	50.44	50.0	–	–	12.30	12.8
% CaO	23.54	24.2	35.48	35.1	45.94	45.5
% Na_2O	26.02	25.1	19.61	19.3	12.69	12.1
% P_2O_5	–	–	44.91	45.1	29.07	29.0
% MnO	–	<0.01	–	<0.01	–	<0.01
% MgO	–	0.08	–	0.05	–	0.05
% TiO_2	–	0.03	–	0.01	–	0.03
% Al_2O_3	–	0.07	–	0.05	–	0.09
% K_2O	–	0.05	–	0.03	–	0.05
% Fe_2O_3	–	0.03	–	0.02	–	0.03
[a]LOI	–	0.43	–	0.33	–	0.34

[a] Loss on ignition (1000 °C).

indicates that the synthesis procedure was successfully performed. In the case of $Ca_5(PO_4)_3OH$, a Ca/P molar ratio of about 1.65 was observed, indicating the stoichiometric phase.

Fig. 1 shows the X-ray diffraction patterns of the samples, confirming their crystalline nature and the success of the synthesis procedure with the formation of the desired phases in isolated form. All the peaks in the diffractograms match those in the standard PDF #77–2189 and PDF #29–1193 sheets of $Na_2CaSi_2O_6$ and β-$NaCaPO_4$, respectively. The diffractogram of β-$NaCaPO_4$−SiO_2 exhibited some noise and a broadening of the peaks in the region of 33°(2θ) compared with that of the pure β-$NaCaPO_4$ because of the incorporation of SiO_2 into its structure. Hence, this compositional change was not sufficient to promote the formation of a new phase — a result that led us to start a crystallographic study to describe it in detail in another study. The diffractogram of the commercial hydroxyapatite also agreed with the standard PDF #84–1998 sheet of $Ca_5(PO_4)_3OH$, as expected.

The FTIR spectra of β-$NaCaPO_4$ and β-$NaCaPO_4$−SiO_2, shown in Fig. 2, are characterized mainly by the presence of signals related to phosphate groups (PO_4^{3-}), whose crystalline nature leads to the splitting

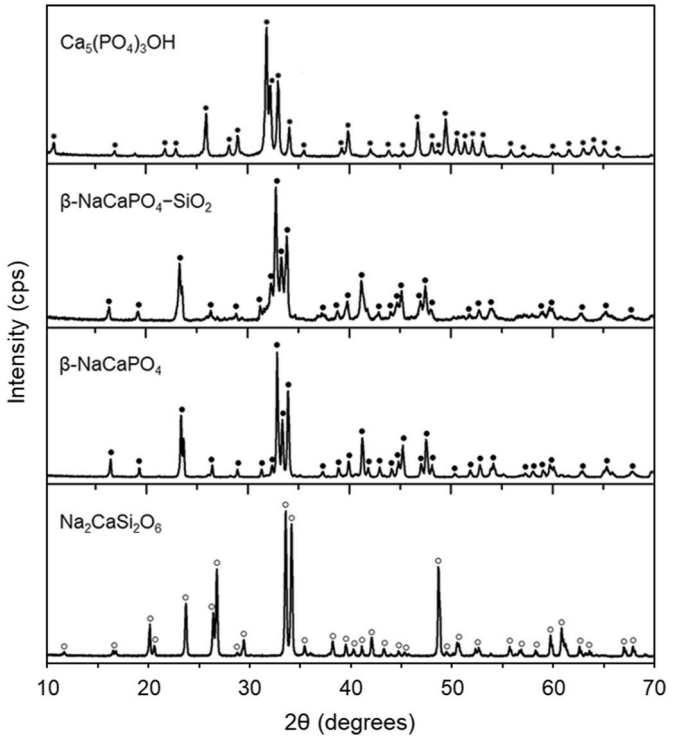

Fig. 1. XRD diffraction patterns of the samples: ○ = $Na_2CaSi_2O_6$ (PDF#77–2189), ● = β-$NaCaPO_4$/β-$NaCaPO_4$−SiO_2 (PDF#29–1193), and ✱ = $Ca_5(PO_4)_3OH$ (PDF#84–1998).

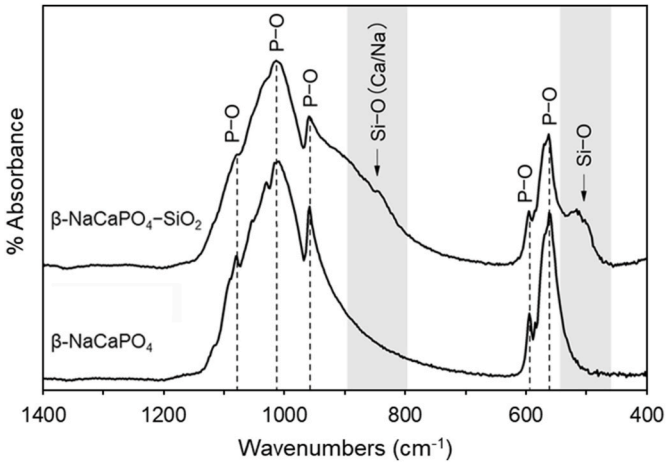

Fig. 2. FTIR spectra of the samples β-$NaCaPO_4$ and β-$NaCaPO_4$−SiO_2.

of some bands. The low-intensity bands that appear as a shoulder at 1078 and 1029 cm^{-1} and the intense band at ~1012 cm^{-1} are associated with asymmetric stretching vibrations of the P–O bond [38,39]. The band located at 958 cm^{-1} is attributed to symmetric stretching vibrations of the P–O bond, while those at 596 and 563 cm^{-1} are due to the O–P–O bond bending [38,39].

The β-$NaCaPO_4$−SiO_2 spectrum shows deformation compared with that of β-$NaCaPO_4$, reinforcing the XRD analysis data discussed previously and confirming the incorporation of silicon into its structure. The bands associated with vibrational phospho-oxygen in PO_4^{3-} and those due to silico-oxygen in SiO_4^{4-} appear practically in the same range of the mid-infrared spectrum (4000-400 cm^{-1}) [10,38,39]. This overlap led to a reduction in the intensity of all absorption bands related to the P–O bond, and a broadening occurred in the spectrum at around 850 cm^{-1} as new signals attributed to the asymmetric stretching of non-bridging oxygen in Si–O(Ca/Na) bonds [10,13,20,38]. Also, the HPO_4^{2-} signal referring to the non-stoichiometric apatitic structure may appear in this same region as a result of the replacement of P^{5+} with Si^{4+} in the crystal lattice. This substitution is non-isoelectric and there is also a difference in the ionic radii and unit cells of the elements involved [33], factors that together can cause considerable change in the structure of the material, as observed in the FTIR spectrum and in the diffractogram shown in Fig. 1. An extra vibrational band, which is characteristic of silicate compounds, appears in the region of 510 cm^{-1}, and is associated with the Si–O bond bending [10,13,20,40].

3.2. Antibacterial activity

The $Na_2CaSi_2O_6$ sample showed an inhibitory effect with the highest concentration (24 mg/mL) established by the agar dilution method, as

Table 2
MIC (mg/mL) values found for the evaluated samples.

Sample	*P. aeruginosa* (ATCC 27853)	*S. aureus* (ATCC 25923)	*S. epidermidis* (ATCC 12228)
[a]Positive control	>0.002	0.0005	>0.002
$Na_2CaSi_2O_6$	24	24	24
β-$NaCaPO_4$	>24	>24	>24
β-$NaCaPO_4$−SiO_2	>24	>24	>24
$Ca_5(PO_4)_3OH$	>24	>24	>24

[a] Positive control = tetracycline.

shown in Table 2. The inhibitory effect on these bacteria was already shown in the literature for other materials with similar compositions [9,10,24,41], in amorphous or crystalline form. This comparison is only qualitative, as different methods and types of bacterial strains were used in these studies, but it reinforces the intrinsic antibacterial activity of materials with compositions close to that of 45S5 bioactive glass, with or without certain concentrations of phosphorus.

None of the other samples exhibited antibacterial activity in the assessed concentration range of 0.5 and 24 mg/mL. For the negative control, antibacterial activity observation was not expected because it was used to ensure that there was no significant external interference in the culture medium and that the inhibitory effect was caused only by the evaluated samples. In the case of phosphate samples, the cause of non-activity may be their low solubility in aqueous medium. According to Ramselaar et al. [42], the *in vitro* solubility of β-$NaCaPO_4$ at pH 7, based on experimental dissolution in distilled water, is ~1.00 mg/mL, while $Ca_5(PO_4)_3OH$ has a solubility of ~0.13 mg/mL (theoretically estimated). Although $Ca_5(PO_4)_3OH$ is practically insoluble, as also reported by other authors [43–46] using different measurement methods and under different condition, even for β-$NaCaPO_4$ which has higher solubility (comparing both phosphates), concentrations up to 24 mg/mL were used attempting to supersaturate the medium, but this strategy had no effect. In addition, no significant difference was observed between the surface areas of these materials, an aspect that also did not influence the assay. Regarding the low tetracycline concentration values, they were established because tetracycline is a well-known antibiotic with a broad action spectrum [47], and it was used as a positive control of the method to confirm bacterial death, as verified for *S. aureus*. In the assay, the other bacteria exhibited greater resistance to this antibiotic (at a concentration of 2×10^{-3} mg/mL) compared with that of *S. aureus*, requiring higher concentrations to observe its effect. The greater resistance of these bacteria against the positive control was also reflected in the samples because the materials tested are not antibiotic in nature, and exhibiting certain antibacterial activity is a highly desired extra feature for medical and dental applications, as they can reduce the use of antibiotics and, simultaneously, aid the repair of infected tissue.

Table 3 shows the results of the direct contact assay. For *P. aeruginosa*, there was a statistical difference between the samples, indicating the positive activity of the evaluated materials against this bacterium. β-$NaCaPO_4$−SiO_2 was able to zero the concentration of viable cells after 5 min of direct contact with the microorganism, while no significant difference was observed for the other samples across the test times, suggesting that the rapid action of the materials after 1 min remained over time compared with the initial bacterial count, before contact is established (0 min). Similar results were also found for the Gram-positive *S. aureus* and *S. epidermidis*, but it seems that these types of bacteria present greater resistance than the Gram-negative *P. aeruginosa*. More clearly, Hu and coauthors [41] demonstrated a difference in the antibacterial activity of Bioglass® against Gram-negative (*Escherichia coli*) and Gram-positive (*S. aureus* and *S. epidermidis*) bacteria, and this observation was associated with their distinct cell walls.

Gram-negative bacteria have a relatively thin (<10 nm) cell wall that is composed mostly of phospholipids, lipopolysaccharides, and proteins, whereas Gram-positive bacteria possess a thick (30–100 nm) outer cell wall composed mainly of peptidoglycan [48,49]. These differences in the cell envelope may provide these bacteria with distinct properties, particularly responses to external stresses, indicating that further investigation is needed to understand better and explain more comprehensively the mechanism of action of the evaluated and similar materials.

A certain reduction in CFU/mL occurred for the inoculum during the assays but the exclusive activity of the materials could be observed by the significant difference ($p < 0.05$) found between the inoculum control and the tested materials, especially for β-$NaCaPO_4$−SiO_2, as previously mentioned. For this sample, the number of viable cells drastically reduced after 5 min in the direct contact test. Earlier studies addressing other materials and bacteria have reported similar results [9,10], but with measurements starting after 10 min — perhaps, an analogous effect can also be achieved in shorter testing times using the same methodology.

Except for β-$NaCaPO_4$−SiO_2, whose result showed strong evidence of its antibacterial effect when in close contact with the bacteria, no statistically significant differences ($p > 0.05$) were found for the other materials. This was not expected for $Ca_5(PO_4)_3OH$ because of its high stability in aqueous medium compared with that of other phosphates. Therefore, in principle, it could not show results comparable to those of $Na_2CaSi_2O_6$, a material that had already shown some activity in the agar dilution assay. Normally, hydroxyapatite exhibits considerable

Table 3
Mean (log) of bacterial growth (CFU/mL) in the direct contact assay for the evaluated samples.

Bacterium	Sample	Contact time				
		0 min	1 min	5 min	10 min	60 min
P. aeruginosa ATCC 27853)	[a]Inoculum control	7.09 ± 0.12	6.38 ± 0.31	6.47 ± 0.41	6.48 ± 0.36	6.60 ± 0.48
	$Na_2CaSi_2O_6$	7.09 ± 0.12	4.84 ± 0.04	4.81 ± 0.03	4.79 ± 0.37	4.22 ± 0.05
	β-$NaCaPO_4$	7.09 ± 0.12	3.28 ± 0.05	4.14 ± 0.06	4.33 ± 0.53	5.08 ± 0.10
	β-$NaCaPO_4$−SiO_2	7.09 ± 0.12	4.02 ± 0.00	0.00 ± 0.00	0.00 ± 0.00	0.00 ± 0.00
	$Ca_5(PO_4)_3OH$	7.09 ± 0.12	5.32 ± 0.02	4.80 ± 0.10	4.21 ± 0.04	4.18 ± 0.02
S. aureus (ATCC 25923)	Inoculum control	6.33 ± 0.21	5.84 ± 0.10	5.89 ± 0.14	6.10 ± 0.11	6.04 ± 0.01
	$Na_2CaSi_2O_6$	6.33 ± 0.21	4.30 ± 0.12	4.56 ± 0.34	4.44 ± 0.57	4.26 ± 0.19
	β-$NaCaPO_4$	6.33 ± 0.21	4.56 ± 0.33	4.61 ± 0.33	4.59 ± 0.40	4.41 ± 0.09
	β-$NaCaPO_4$−SiO_2	6.33 ± 0.21	3.30 ± 0.35	0.00 ± 0.00	0.00 ± 0.00	0.00 ± 0.00
	$Ca_5(PO_4)_3OH$	6.33 ± 0.21	5.17 ± 0.24	5.26 ± 006	4.94 ± 0.05	4.38 ± 0.21
S. epidermidis (ATCC 12228)	Inoculum control	5.79 ± 0.43	5.36 ± 0.21	5.42 ± 0.09	5.43 ± 0.09	5.55 ± 0.02
	$Na_2CaSi_2O_6$	5.79 ± 0.43	4.08 ± 0.11	3.90 ± 0.14	3.92 ± 0.17	3.95 ± 0.03
	β-$NaCaPO_4$	5.79 ± 0.43	3.95 ± 0.23	4.13 ± 0.28	4.02 ± 0.27	4.14 ± 0.13
	β-$NaCaPO_4$−SiO_2	5.79 ± 0.43	2.99 ± 0.09	0.00 ± 0.00	0.00 ± 0.00	0.00 ± 0.00
	$Ca_5(PO_4)_3OH$	5.79 ± 0.43	5.14 ± 0.02	4.82 ± 0.12	3.77 ± 0.10	3.36 ± 0.25

[a] Inoculum control = culture medium + bacteria.

antibacterial activity when on a nanoscale [50] or when containing some element with recognized activity in its structure, such as silver and zinc [1–3,12]. Likewise, for materials that already show a certain activity, such as Bioglass®, nanometric powders can provide an increase in this property [51]. Thus, as undoped particulate materials were evaluated on a micrometric scale (<50 μm), it is reasonable that some unknown experimental conditions, unfavorable for bacteria, may have contributed to the reduction in viable cells observed for $Ca_5(PO_4)_3OH$. However, for our initial purpose, these results were enough to show the comparative effect of the tested materials against the potential skin pathogenic bacteria, especially β-$NaCaPO_4$−SiO_2.

Concerning the possible reasons that led to damage and reduction of this bacterial count in the direct contact method related to the material evaluated, the increase in pH and osmolarity in the surrounding environment can be mentioned [10,32,35,41,51,52]. Debris released from the materials in the medium may also have had a certain influence [41]. To verify the effect of pH, its variation caused by the samples was measured in a condition similar to that of the assay. The data shown in Fig. 3 indicate a rapid increase in the pH value in the initial times, remaining globally stable until the last measured time (60 min).

The samples led to an increase in pH essentially by releasing some ions (Na^+/Ca^{2+}) with their partial dissolution. Waltimo et al. [51] also demonstrated a significant increase in pH with a contribution from dissolved silica (SiO_2), which interfered in the acid-base equilibria of the medium by means of its successive de/re-protonation. These data help justify the greater pH variation observed for the β-$NaCaPO_4$−SiO_2 sample, due to the silica that can be released from its composition. As the $Na_2CaSi_2O_6$ sample released almost the same species in the medium, it probably had a different degradability rate — a parameter that was not investigated in this study. The lowest pH variation observed for the $Ca_5(PO_4)_3OH$ sample was due to its higher stability (low degradability) in the medium, reaching a maximum value of ~8.8. The abrupt change occurred in the first minute and the pH value reached was practically constant over time. For the other samples, the general variation trend was similar, with the maximum values reached for $Na_2CaSi_2O_6$, β-$NaCaPO_4$, and β-$NaCaPO_4$−SiO_2 equal to ~10.7, 10.1, and 11.8, respectively. The increase in pH seems to play a role in the antibacterial activity of these materials because the significant reduction in the bacterial count shown in Table 3 occurred in the assays of 1 and 5 min, the same times at which pH presented its greater variation. In addition, the material that presented the strongest bactericidal effect (β-$NaCaPO_4$−SiO_2), eliminating all the assessed bacteria, was the same that had the greatest pH variation. Although the difference in pH caused by β-$NaCaPO_4$−SiO_2 and $Na_2CaSi_2O_6$ was only ~1.1, this value is significant because pH was presented on a log scale. Therefore, the change in hydroxyl ions (OH^-) in the medium becomes relevant, as shown in Table 4.

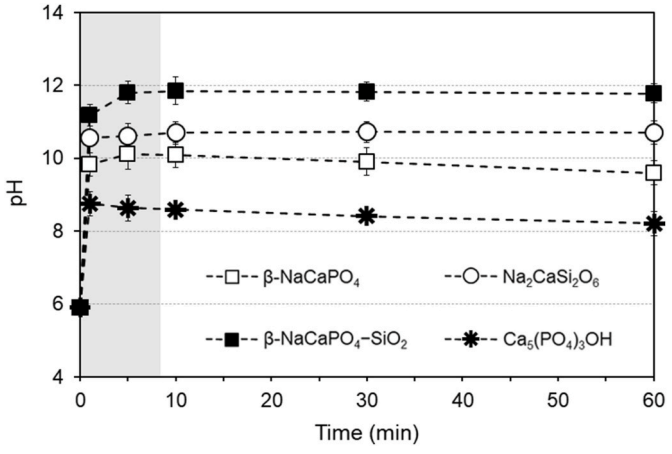

Fig. 3. Variations in pH caused by the samples as a function of immersion time in 0.9% NaCl solution.

A high concentration of hydroxyl ions in the medium can damage bacterial cells through different mechanisms [53]. Thus, the contribution of this pH variation to the antibacterial effect shown by the samples cannot be ruled out. Moreover, it is also important to mention the ions released from the samples because of their partial solubilities. Calcium ions, for example, in addition to altering the pH, can kill bacteria by destabilizing their cell membranes [54,55]. The release of silica, which is also associated with an increase in pH and a high alkaline buffer capacity [51], can establish, together with calcium, a good disinfectant system. Since measuring pH variation is only an indirect way of accessing the rate of sample degradation, it is necessary to conduct a study to monitor the dissolution of materials in a simulated environment to discriminate which ions and concentrations released from each sample will be capable of causing damage to a particular bacterium.

3.3. Keratinocyte and stem cell viability

Although the MTT assay evaluates the cell metabolic activity, this test is extensively used as a cell viability assessment, as indicated by ISO 10993–5:2009, Biological evaluation of medical devices — Part 5: Tests for *in vitro* cytotoxicity (in annex C). Additionally, ISO 10993–5:2009 mentions that if cell viability is reduced to <70% of the blank, the evaluated material has a cytotoxic potential indicated by the MTT assay because a decrease in the number of living cells results in a reduction in the metabolic activity in the sample. Thus, the results of the MTT assay related to the viability of keratinocytes are shown in Fig. 4, and they indicate that no sample tested exhibited cytotoxicity. The control, which consisted of untreated cells for reference, was taken as 100% on the *y* axis and the viability of the cells treated with the samples was expressed as the percentage of control. Statistical difference in the relative cell viability was observed when the keratinocytes were treated with β-$NaCaPO_4$−SiO_2 ($p = 0.0193$). Regarding concentration, a significant difference was found only when the HaCaT cells were treated with the β-$NaCaPO_4$−SiO_2 sample at 1.0 mg/mL but without showing any substantial activity, as indicated in Fig. 4C. Nevertheless, all data reveal an *in vitro* tolerance of the human keratinocytes in direct contact with the other concentrations and samples tested, without showing cytotoxicity. This is an important finding because keratinocytes are the major cell type present in the epidermis, which can produce cellular and structural extracellular matrix proteins, such as filaggrin, involucrin, loricrin, and keratins [56]. Remodeling keratin cytoskeleton, for example, is important for cell-cell and cell-matrix adhesion, processes that are fundamental for cell motility during wound healing or inflammation [57].

When studying fibrous polymer scaffolds with potential use for skin replacement, Girón and coauthors [37] reported a considerable increase in keratinocyte viability between 1 and 6 days of incubation, indicating that a longer induction time is needed for these cells to show appreciable activity. This is an issue that should be verified for the bioceramics tested here in a more specific and in-depth investigation. In one of the few published studies on the viability and growth of HaCaT cells exposed to a related material [58], granules of S53P4 bioactive glass ($53SiO_2$–$20CaO$–$23Na_2O$–$4P_2O_5$, by wt%) with size ranging from 0.5 to

Table 4
Molar concentration of hydroxyl ions related to pH variation (average) caused by the samples.

Time (min)	$Na_2CaSi_2O_6$ [OH^-]	β-$NaCaPO_4$ [OH^-]	β-$NaCaPO_4$−SiO_2 [OH^-]	$Ca_5(PO_4)_3OH$ [OH^-]
0	7.76×10^{-9}	7.76×10^{-9}	7.76×10^{-9}	7.76×10^{-9}
1	3.63×10^{-4}	6.76×10^{-5}	1.51×10^{-3}	5.62×10^{-6}
5	3.98×10^{-4}	1.25×10^{-4}	6.30×10^{-3}	4.46×10^{-6}
10	5.01×10^{-4}	1.23×10^{-4}	6.76×10^{-3}	3.98×10^{-6}
30	5.24×10^{-4}	7.76×10^{-5}	6.45×10^{-3}	2.51×10^{-6}
60	5.12×10^{-4}	3.80×10^{-5}	5.88×10^{-3}	1.65×10^{-6}

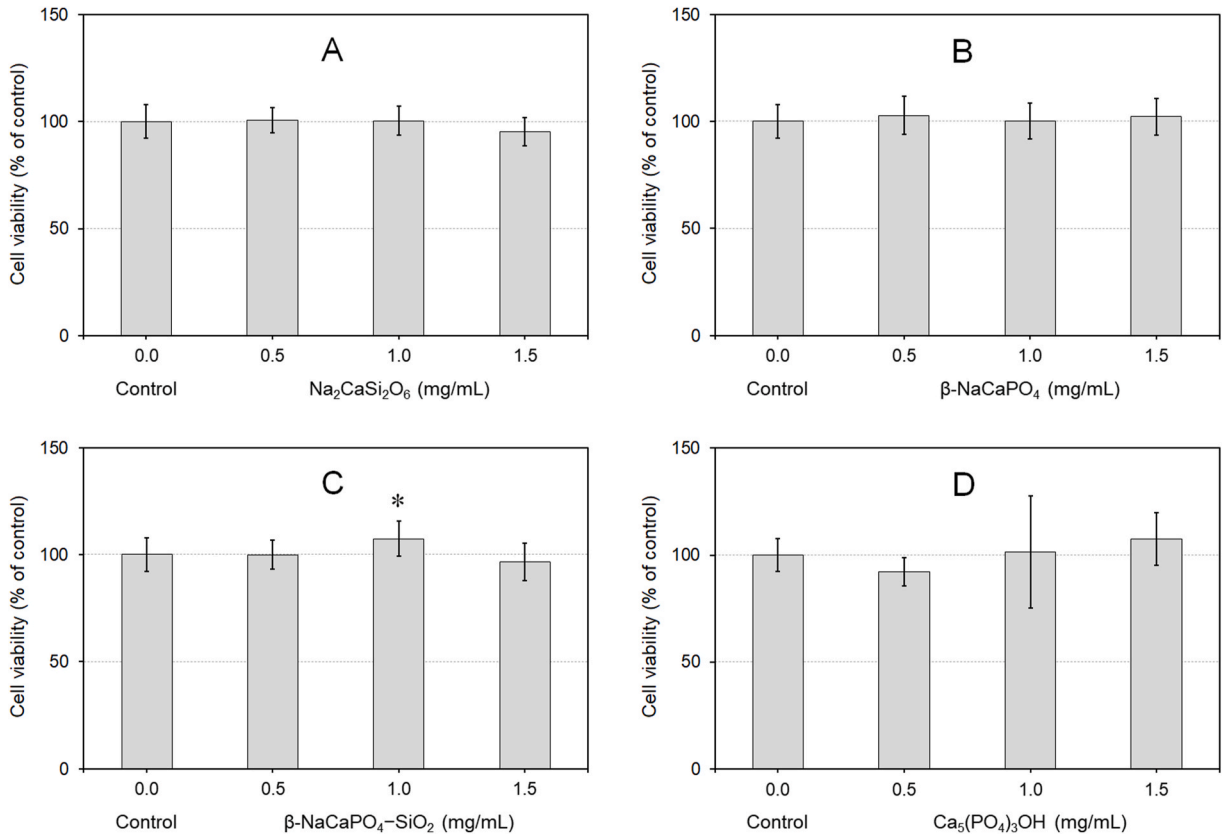

Fig. 4. Effect of samples on the viability of keratinocytes measured by the MTT assay after 1 day: A) sodium calcium silicate, B) beta-rhenanite, C) beta-rhenanite modified with silicon, and D) hydroxyapatite. Data are presented as mean ± SD of the percentage of control, where * indicates $p < 0.05$ *vs.* control.

0.8 mm were incubated in different cell culture media for 6 days, with the cell viability determined by the MTT method after 2 days of incubation. The tested cell culture media, DMEM and keratinocyte growth medium (KGM), became increasingly alkaline when subjected to incubation with the S53P4 bioactive glass granules, changing from 7.74 to 8.01 and from 7.63 to 8.61 after 6 days, respectively, with 10% granule concentrations. The HaCaT cell viability decreased when the material was incubated in KGM but not in DMEM. According to those authors, the cause of the reduced HaCaT viability observed could be pH-dependent, and the differences in the results between the groups may be associated with the distinct constitutions of each culture medium, which are not disclosed in detail by the manufacturers. Overall, along with cell culture microscopy, medium cytokine profile, and scratch assay, they concluded that the S53P4 bioactive glass seemed to have an inhibitory effect on HaCaT cell growth, and although further studies are needed, this property may favor the treatment of cholesteatoma, which is an inflammatory, destructive, and locally invasive middle ear lesion composed of proliferative keratinizing squamous epithelium and its subepithelial connective tissue [58,59].

Fig. 5 shows the interaction between the materials and stem cells. Again, cytotoxicity was not observed and, in general, the materials induced greater activity of stem cells compared with keratinocytes (Fig. 4). In contrast to what was observed for keratinocytes, there was a statistically significant difference, indicating an increase in cell viability in relation to the control when the stem cells were treated with β-$NaCaPO_4$–SiO_2 ($p < 0.0001$) at the three concentrations tested. This cell type was more sensitized by the samples, a result that is not abnormal because different cell types can respond differently to a bioactive material when both are conditioned together [60]. This fact may even trigger certain specific pathways to designate the developed material since its degradability and, consequently, ionic products released in physiological conditions are responsible to provide stimuli to several biological processes [5,11]. As the effect caused by the material on the body can be influenced by time and in a dose-dependent manner according to its rate of degradation, it is extremely important to design and adjust the material chemistry to produce matrices as potential transport systems for the controlled release of ions that assist with tissue regeneration.

The interesting point that stands out in this assay is that there was a statistical difference between the samples, in which the β-$NaCaPO_4$–SiO_2 sample affects the stem cell viability in a dose-dependent manner, as illustrated in Fig. 5C. It seems that the silicon content of this sample contributes to the greater response observed in stem cell viability compared with those of the other evaluated materials, mainly β-$NaCaPO_4$ and $Ca_5(PO_4)_3OH$. In addition to the influence on antibacterial activity, discussed earlier, silicon can also promote significantly positive effects on the biological properties of calcium phosphates, with Si-doped material capable of inducing higher *in vitro* bioactivity, cell viability and attachment, and bone mineralization ability [1,2,11,61]. It is not surprising that the effects of silicon compounds on biomineralization, osteogenesis, and tissue formation have been widely investigated [62,63]. Hence, the known or proposed role played by silicon in materials, intended to assist with the regeneration of different tissues, is the basis for its use as an element in biomaterials research.

In this study, the possible positive effects of silicon species released from the evaluated samples are considered qualitative because they were not measured and no direct correlation between this element (and any other) and the biological performance observed for the materials was investigated. It is recognized that different compositions and structures interfere with material degradability, a fact that helps explain the results found for each sample. Consequently, the release profile of components, including silicon, will be characteristic of each material, as in the case of $Na_2CaSi_2O_6$ and β-$NaCaPO_4$–SiO_2, which are samples that behaved differently in the experiments even though both contain silicon.

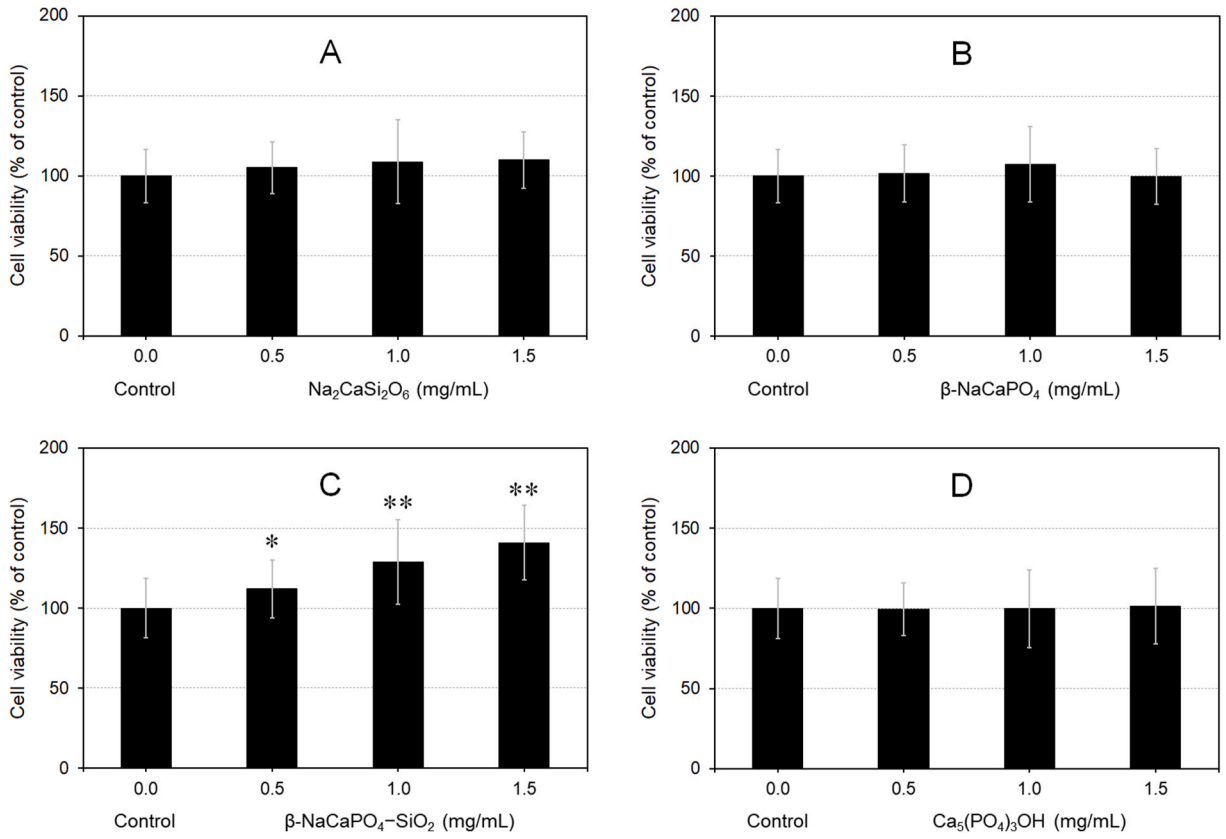

Fig. 5. Effect of samples on the stem cell viability measured by the MTT assay after 1 day: A) sodium calcium silicate, B) beta-rhenanite, C) beta-rhenanite modified with silicon, and D) hydroxyapatite. Data are presented as mean ± SD of the percentage of control, where * indicates $p < 0.05$ and ** $p < 0.01$ *vs.* control.

For this reason, the degradability and ion release profile of some samples should be studied to better understand their mechanisms of action, thus enabling direct modifications for more specific and efficient applications.

Regarding the effect of increased pH on cell viability, the measurement shown in Fig. 6 indicates that a medium with high alkalinity exhibits cytotoxicity (significantly reduces cell viability). In the example in Fig. 6, the control group used in experiments was compared with stem cells cultivated in a medium added with 0.46 M NaOH, resulting initially in a pH value close to 14. After 24 h, the pH value decreased to about 10 in the culture conditions and the relative cell viability decreased significantly compared with that of the cells cultivated in the unmodified medium, used as control ($p < 0.0001$).

Although the β-$NaCaPO_4$–SiO_2 sample increased the pH value to ~12 in the test shown in Fig. 3, the pH value was not affected in the same way in the test involving the culture of stem cells, because it was buffered with sodium bicarbonate and HEPES, which are biological buffer agents that function over a pH range of approximately 6.8–8.2. With these components, the medium pH is equilibrated in the incubator following the standard condition (5% CO_2 in humidified air and 37 °C) and, as a result, the pH values do not change sharply. As shown in Fig. 7, the pH value started at 7.86 for the control and 7.96 for the culture medium with 1.5 mg/mL β-$NaCaPO_4$–SiO_2 and remained stable for the first 60 min, which is the most critical period because of the greater

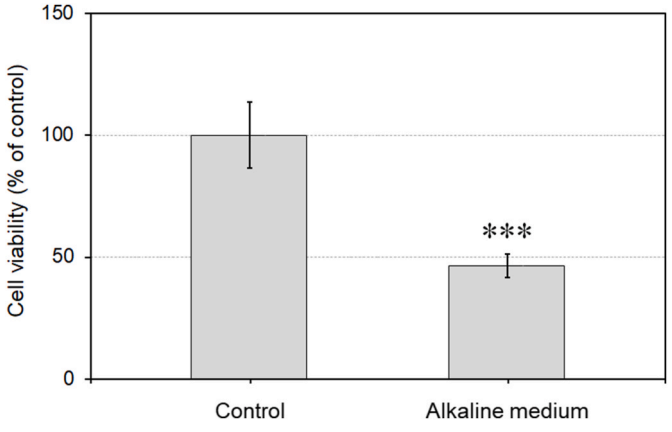

Fig. 6. Effect of alkaline medium on the stem cell viability measured by the MTT assay after 24 h. Data are presented as mean ± SD of the percentage of control, where *** indicates $p < 0.0001$ *vs.* control by the *t*-test.

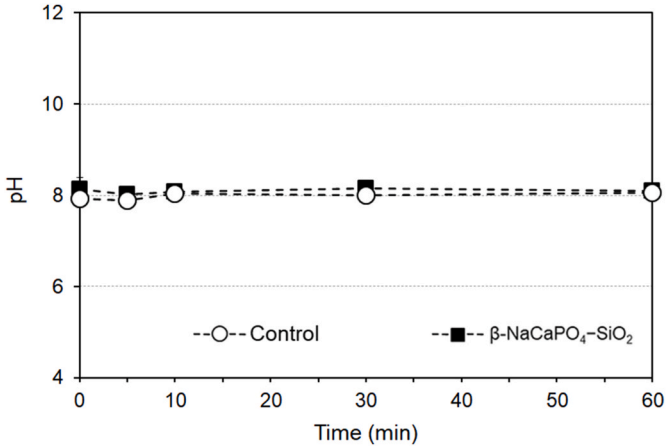

Fig. 7. Values of pH provided by the control and 1.5 mg/mL β-$NaCaPO_4$–SiO_2 as a function of immersion time in the *in vitro* stem cell cultivated conditions.

release of ions from the sample to the medium until the system reaches a certain equilibrium. After 24 h, the pH values hardly changed, staying at ~7.74 and 7.77 for the control and the culture medium, respectively. Although no significant pH variation was observed in the culture medium during our experiment, in addition to the influence of different culture media and materials employed for the purpose [35,58], there could be a level of alkalinity that specific cells in the environment can tolerate. Thus, as previously mentioned, it is necessary to incubate keratinocytes for a longer period to observe more accurately their response when in direct contact with the material and, consequently, guide some potential applications.

4. Conclusions

In this study, the main crystalline $Na_2CaSi_2O_6$, β-$NaCaPO_4$, and β-$NaCaPO_4$−SiO_2 phases formed by crystallization of the 45S5 bioactive glass were successfully synthesized in particulate form by a simple, reproducible, solid-state reaction method. The β-$NaCaPO_4$−SiO_2 phase exhibited the best antibacterial effects against *Pseudomonas aeruginosa*, *Staphylococcus aureus*, and *S. epidermidis*, fact attributed to the more alkaline microenvironment generated when compared with the other samples, and perhaps to the ions released to the medium (although this last parameter has not been quantified). The cell metabolic activity of human stem cells and keratinocytes treated with this silica-phosphate phase was also higher than that of other evaluated materials, including a commercial sample of hydroxyapatite, which is one of the most used bioceramics. This positive performance of the tested materials warrants more specific studies to assess their degradability profile and keratinocyte viability and proliferation in detail. The β-$NaCaPO_4$−SiO_2 phase seems to be especially promising to assist in tissue engineering — in combination with other materials or as a standalone material — with the possibility of over-performing hydroxyapatite in some applications.

Declaration of competing interest

The authors declare that they have no known competing financial interests or personal relationships that could have appeared to influence the work reported in this paper.

Acknowledgments

The materials were developed, synthesized, and physicochemically characterized using RLS's resources, with no funding from any government or private institutions. For biological characterization, the authors would like to acknowledge the support of the Brazilian agencies CAPES, CNPq, IPCT, INCT-REGENERA, MCTIC (grant no. #23078.010846/2019–78), FINEP (grant no. #0114013500), and FAPERGS (grant no. #17/255/0001271–2). NM also thanks CNPq for fellowship (PDS, grant no. #101379/2022–6). EDZ is grateful to the FAPESP (CEPID, grant no. #13/007793–6).

References

[1] B. Ghiasi, Y. Sefidbakht, S. Mozaffari-Jovin, B. Gharehcheloo, M. Mehrarya, A. Khodadadi, M. Rezaei, S.O.R. Siadat, V. Uskoković, Hydroxyapatite as a biomaterial — a gift that keeps on giving, Drug Dev. Ind. Pharm. 46 (2020) 1035–1062, https://doi.org/10.1080/03639045.2020.1776321.

[2] V.G. DileepKumar, M.S. Sridhar, P. Aramwit, V.K. Krut'ko, O.N. Musskaya, I. E. Glazov, N. Reddy, A review on the synthesis and properties of hydroxyapatite for biomedical applications, J. Biomater. Sci. Polym. Ed. 33 (2022) 229–261, https://doi.org/10.1080/09205063.2021.1980985.

[3] D.G. Filip, V.-A. Surdu, A.V. Paduraru, E. Andronescu, Current development in biomaterials — hydroxyapatite and bioglass for applications in biomedical field: a review, J. Funct. Biomater. 13 (2022) 1–21, https://doi.org/10.3390/jfb13040248.

[4] V. Miguez-Pachecoa, L.L. Henchb, A.R. Boccaccini, Bioactive glasses beyond bone and teeth: emerging applications in contact with soft tissues, Acta Biomater. 13 (2015) 1–15, https://doi.org/10.1016/j.actbio.2014.11.004.

[5] U. Pantulap, M. Arango-Ospina, A.R. Boccaccini, Bioactive glasses incorporating less-common ions to improve biological and physical properties, J. Mater. Sci. Mater. Med. 3 (2022) 1–41, https://doi.org/10.1007/s10856-021-06626-3.

[6] L.L. Hench, The story of Bioglass®, J. Mater. Sci. Mater. Med. 17 (2006) 967–978, https://doi.org/10.1007/s10856-006-0432-z.

[7] J. Deubener, M. Allix, M.J. Davis, A. Duran, T. Höche, T. Honma, T. Komatsu, S. Krüger, I. Mitra, R. Müller, S. Nakane, M.J. Pascual, J.W.P. Schmelzer, E. D. Zanotto, S. Zhou, Updated definition of glass-ceramics, J. Non-Cryst. Solids 501 (2018) 3–10, https://doi.org/10.1016/j.jnoncrysol.2018.01.033.

[8] M. Cannio, D. Bellucci, J.A. Roether, D.N. Boccaccini, V. Cannillo, Bioactive glass applications: a literature review of human clinical trials, Materials 14 (2021) 1–25, https://doi.org/10.3390/ma14185440.

[9] C.H.G. Martins, T.C. Carvalho, M.G.M. Souza, C. Ravagnani, O. Peitl, E.D. Zanotto, H. Panzeri, L.A. Casemiro, Assessment of antimicrobial effect of Biosilicate® against anaerobic, microaerophilic and facultative anaerobic microorganisms, J. Mater. Sci. Mater. Med. 22 (2011) 1439–1446, https://doi.org/10.1007/s10856-011-4330-7.

[10] R.L. Siqueira, P.F.S. Alves, T. da Silva Moraes, L.A. Casemiro, S.N. da Silva, O. Peitl, C.H.G. Martins, E.D. Zanotto, Cation-doped bioactive ceramics: *in vitro* bioactivity and effect against bacteria of the oral cavity, Ceram. Int. 45 (2019) 9231–9244, https://doi.org/10.1016/j.ceramint.2019.02.001.

[11] X. Wang, M. Tang, Bioceramic materials with ion-mediated multifunctionality for wound healing, Smart Med 1 (2022) 1–15, https://doi.org/10.1002/SMMD.20220032.

[12] M. Riaz, R. Zia, A. Ijaz, T. Hussain, M. Mohsin, A. Malik, Synthesis of monophasic Ag doped hydroxyapatite and evaluation of antibacterial activity, Mater. Sci. Eng. C 90 (2018) 308–313, https://doi.org/10.1016/j.msec.2018.04.076.

[13] O. Peitl, E.D. Zanotto, L.L. Hench, Highly bioactive P_2O_5–Na_2O–CaO–SiO_2 glass-ceramics, J. Non-Cryst. Solids 292 (2001) 115–126, https://doi.org/10.1016/S0022-3093(01)00822-5.

[14] C.-C. Lin, L.-C. Huang, P. Shen, $Na_2CaSi_2O_6$–P_2O_5 based bioactive glasses. Part 1: elasticity and structure, J. Non-Cryst. Solids 351 (2005) 3195–3203, https://doi.org/10.1016/j.jnoncrysol.2005.08.020.

[15] L. Lefebvre, J. Chevalier, L. Gremillard, R. Zenati, G. Thollet, D. Bernache-Assolant, A. Govin, Structural transformations of bioactive glass 45S5 with thermal treatments, Acta Mater. 55 (2007) 3305–3313, https://doi.org/10.1016/j.actamat.2007.01.029.

[16] G.K. Moir, F.P. Glasser, Phase equilibria in the system Na_2SiO_3–$CaSiO_3$, Phys. Chem. Glasses 15 (1974) 6–11.

[17] A.R. El-Ghannam, Advanced bioceramic composite for bone tissue engineering: design principles and structure-bioactivity relationship, J. Biomed. Mater. Res. 69 (2004) 490–501, https://doi.org/10.1002/jbm.a.30022.

[18] A. El-Ghannam, C.Q. Ning, J. Mehta, Cyclosilicate nanocomposite: a novel resorbable bioactive tissue engineering scaffold for BMP and bone-marrow cell delivery, J. Biomed. Mater. Res. 71 (2004) 377–390, https://doi.org/10.1002/jbm.a.30128.

[19] X. Liu, A. El-Ghannam, Effect of processing parameters on the microstructure and mechanical behavior of silica-calcium phosphate nanocomposite, J. Mater. Sci. Mater. Med. 21 (2010) 2087–2094, https://doi.org/10.1007/s10856-010-4062-0.

[20] R.L. Siqueira, E.D. Zanotto, Facile route to obtain a highly bioactive SiO_2–CaO–Na_2O–P_2O_5 crystalline powder, Mater. Sci. Eng., C 31 (2011) 1791–1799, https://doi.org/10.1016/j.msec.2011.08.013.

[21] A.T.C. Jaimes, A. Pablos-Martín, K. Hurle, J.M.S. Silva, L. Berthold, T. Kittel, A. R. Boccaccini, D.S. Brauer, Deepening our understanding of bioactive glass crystallization using TEM and 3D nano-CT, J. Eur. Ceram. Soc. 41 (2021) 4958–4969, https://doi.org/10.1016/j.jeurceramsoc.2021.02.051.

[22] G.S. Lázaro, S.C. Santos, C.X. Resende, E.A. Santos, Individual and combined effects of the elements Zn, Mg and Sr on the surface reactivity of a SiO_2·CaO·Na_2O·P_2O_5 bioglass system, J. Non-Cryst. Solids 386 (2014) 19–28, https://doi.org/10.1016/j.jnoncrysol.2013.11.038.

[23] H.C. Li, D.G. Wang, C.Z. Chen, Effect of sodium oxide and magnesia on structure, *in vitro* bioactivity and degradability of wollastonite, Mater. Lett. 135 (2014) 237–240, https://doi.org/10.1016/j.matlet.2014.07.177.

[24] R.L. Siqueira, L.C. Costa, M.A. Schiavon, D.T. Castro, A.C. Reis, O. Peitl, E. D. Zanotto, Bioglass® and resulting crystalline materials synthesized via an acetic acid-assisted sol-gel route, J. Sol. Gel Sci. Technol. 83 (2017) 165–173, https://doi.org/10.1007/s10971-017-4402-3.

[25] S. Chitra, P. Bargavi, D. Durgalakshmi, P. Rajashree, S. Balakumar, Role of sintering temperature dependent crystallization of bioactive glasses on erythrocyte and cytocompatibility, Process. Appl. Ceram. 13 (2019) 12–23, https://doi.org/10.2298/PAC1901012C.

[26] R.R. Chandran, S. Chitra, S. Vijayakumari, P. Bargavi, S. Balakumar, Cognizing the crystallization aspects of $NaCaPO_4$ concomitant 53S bioactive-structures and their imprints in *in vitro* bio-mineralization, New J. Chem. 45 (2021) 15350–15362, https://doi.org/10.1039/D1NJ01058A.

[27] V. Sugumaran, E. Krishnamoorthy, A. Kamalakkannan, R.C. Ramachandran, B. Subramanian, Unscrambling the influence of sodium cation on the structure, bioactivity, and erythrocyte compatibility of 45S5 bioactive glass, ACS Appl. Bio Mater. 5 (2022) 1576–1590, https://doi.org/10.1021/acsabm.1c01322.

[28] R.L. Siqueira, J.H. Alano, O. Peitl, E.D. Zanotto, GlassPanacea: a user-friendly free software tool for the formulation of glasses, glass-ceramics, and ceramics, Am. Ceram. Soc. Bull. 96 (2017) 48–49.

[29] R.L. Siqueira, J.H. Alano, O. Peitl, E.D. Zanotto, GlassPanacea: an efficient software for the formulation of ceramic materials, Quim. Nova 41 (2018) 446–450, https://doi.org/10.21577/0100-4042.20170196.

[30] S. Brunauer, P.H. Emmett, E. Teller, Adsorption of gases in multimolecular layers, J. Am. Chem. Soc. 60 (1938) 309–319, https://doi.org/10.1021/ja01269a023.
[31] J.H. Jorgensen, J.D. Turnidge, Susceptibility test methods: dilution and disk diffusion methods, in: J. Jorgensen, M. Pfaller, K. Carroll, G. Funke, M. Landry, S. Richter, D. Warnock (Eds.), Man. Clin. Microbiol, 11 ed., ASM Press, Washington, 2015.
[32] P. Stoor, E. Söderling, J.I. Salonen, Antibacterial effects of a bioactive glass paste on oral microorganisms, Acta Odontol. Scand. 56 (1998) 161–165, https://doi.org/10.1080/000163598422901.
[33] D.R. Lide, Handbook of Chemistry and Physics, 87th ed., CRC Press, Boca Raton, 2007.
[34] L. Bernardi, S.B. Luisi, R. Fernandes, T.P. Dalberto, L. Valentim, J.A.B. Chies, A.C. M. Fossati, P. Pranke, The isolation of stem cells from human deciduous teeth pulp is related to the physiological process of resorption, J. Endod. 37 (2011) 973–979, https://doi.org/10.1016/j.joen.2011.04.010.
[35] R.L. Siqueira, N. Maurmann, D. Burguêz, D. Pereira, A.N.S. Rastelli, O. Peitl, P. Pranke, E.D. Zanotto, Bioactive gel-glasses with distinctly different compositions: bioactivity, viability of stem cells and antibiofilm effect against *Streptococcus mutans*, Mater. Sci. Eng., C 76 (2017) 233–241, https://doi.org/10.1016/j.msec.2017.03.056.
[36] Y. Liu, D.A. Peterson, H. Kimura, D. Schubert, Mechanism of cellular 3-(4,5-dimethylthiazol-2-yl)-2,5-diphenyltetrazolium bromide (MTT) reduction, J. Neurochem. 69 (1997) 581–593, https://doi.org/10.1046/j.1471-4159.1997.69020581.x.
[37] J. Girón, N. Maurmann, M. Silveira, C.A. Ferreira, P. Pranke, Development of fibrous PLGA/fibrin scaffolds as a potential skin substitute, Biomed. Mater. 15 (2020), 055014, https://doi.org/10.1088/1748-605X/aba086.
[38] H. Aguiar, J. Serra, P. González, B. León, Structural study of sol-gel silicate glasses by IR and Raman spectroscopies, J. Non-Cryst. Solids 355 (2009) 475–480, https://doi.org/10.1016/j.jnoncrysol.2009.01.010.
[39] W. Jastrzębski, M. Sitarz, M. Rokita, K. Bułat, Infrared spectroscopy of different phosphates structures, Spectrochim. Acta Part A Mol. Biomol. Spectrosc. 79 (2011) 722–727, https://doi.org/10.1016/j.saa.2010.08.044.
[40] E.R. Lippincott, A. Van Valkenburg, C.E. Weir, E.N. Bunting, Infrared studies on polymorphs of silicon dioxide and germanium dioxide, J. Res. Natl. Bur. Stand. 61 (1958) (1934) 61–70, https://doi.org/10.6028/jres.061.009.
[41] S. Hu, J. Chang, M. Liu, C. Ning, Study on antibacterial effect of 45S5 Bioglass®, J. Mater. Sci. Mater. Med. 20 (2009) 281–286, https://doi.org/10.1007/s10856-008-3564-5.
[42] M.M.A. Ramselaar, F.C.M. Driessens, W. Kalk, J.R. De Wijn, P.J. Van Mullem, Biodegradation of four calcium phosphate ceramics; *in vivo* rates and tissue interactions, J. Mater. Sci. Mater. Med. 2 (1991) 63–70, https://doi.org/10.1007/BF00703460.
[43] E.C. Moreno, T.M. Gregory, W.E. Brown, Preparation and solubility of hydroxyapatite, J. Res. Natl. Bur. Stand. A Phys. Chem. 72A (1968) 773–782, https://doi.org/10.6028/jres.072A.052.
[44] S.V. Dorozhkin, Calcium orthophosphates ($CaPO_4$): occurrence and properties, Prog. Biomater. 5 (2016) 9–70, https://doi.org/10.1007/s40204-015-0045-z.
[45] Z.-F. Chen, B.W. Darvell, V.W.-H. Leung, Hydroxyapatite solubility in simple inorganic solutions, Arch. Oral Biol. 49 (2004) 359–367, https://doi.org/10.1016/j.archoralbio.2003.12.004.
[46] G. Kuranov, K. Mikhelson, A. Puzyk, Solubility of hydroxyapatite as a function of solution composition (experiment and modeling), in: O.V. Frank-Kamenetskaya, D. Y. Vlasov, E.G. Panova, S.N. Lessovaia (Eds.), Processes and Phenomena on the Boundary between Biogenic and Abiogenic Nature. Lecture Notes in Earth System Sciences, Springer, Cham, 2020, https://doi.org/10.1007/978-3-030-21614-6_3.
[47] G.G. Dhakad, R.V. Patil, D.S. Girase, S.P. Amrutkar, R.S. Jain, Review on antibiotics, Asian J. Res. Chem. 15 (2022) 91–96, https://doi.org/10.52711/0974-4150.2022.00015.
[48] J. Rundegren, T. Sjödin, L. Petersson, E. Hansson, I. Jonsson, Delmopinol interactions with cell walls of Gram-negative and Gram-positive oral bacteria, Oral Microbiol. Immunol. 10 (1995) 102–109, https://doi.org/10.1111/j.1399-302X.1995.tb00127.x.
[49] T.J. Silhavy, D. Kahne, S. Walker, The bacterial cell envelope, Cold Spring Harbor Perspect. Biol. 2 (2010) 1–16, https://doi.org/10.1101/cshperspect.a000414.
[50] S. Lamkhao, M. Phaya, C. Jansakun, N. Chandet, K. Thongkorn, G. Rujijanagul, P. Bangrak, C. Randorn, Synthesis of hydroxyapatite with antibacterial properties using a microwave-assisted combustion method, Sci. Rep. 9 (2019) 1–9, https://doi.org/10.1038/s41598-019-40488-8.
[51] T. Waltimo, T.J. Brunner, M. Vollenweider, W.J. Stark, M. Zehnder, Antimicrobial effect of nanometric bioactive glass 45S5, J. Dent. Res. 86 (2007) 754–757, https://doi.org/10.1177/154405910708600813.
[52] I. Allan, H. Newman, M. Wilson, Antibacterial activity of particulate Bioglass® against supra- and subgingival bacteria, Biomaterials 22 (2001) 1683–1687, https://doi.org/10.1016/S0142-9612(00)00330-6.
[53] J.F. Siqueira, H.P. Lopes, Mechanisms of antimicrobial activity of calcium hydroxide: a critical review, Int. Endod. J. 32 (1999) 361–369, https://doi.org/10.1046/j.1365-2591.1999.00275.x.
[54] J.S. Moya, L. Esteban-Tejeda, C. Pecharromán, S.R.H. Mello-Castanho, A.C. Silva, F. Malpartida, Glass powders with a high content of calcium oxide: a step towards a "green" universal biocide, Adv. Eng. Mater. 13 (2011) B256–B260, https://doi.org/10.1002/adem.201080133.
[55] Y. Xie, L. Yang, Calcium and magnesium ions are membrane-active against stationary-phase *Staphylococcus aureus* with high specificity, Sci. Rep. 6 (2016), 20628, https://doi.org/10.1038/srep20628.
[56] T. Kobiela, M. Milner-Krawczyk, M. Pasikowska-Piwko, K. Bobecka-Wesołowska, I. Eris, W. Święszkowski, I. Dulinska-Molak, The effect of anti-aging peptides on mechanical and biological properties of HaCaT keratinocytes, Int. J. Pept. Res. Therapeut. 24 (2018) 577–587, https://doi.org/10.1007/s10989-017-9648-7.
[57] K. Seltmann, A.W. Fritsch, J.A. Käs, T.M. Magin, Keratins significantly contribute to cell stiffness and impact invasive behavior, Proc. Natl. Acad. Sci. USA 110 (2013) 18507–18512, https://doi.org/10.1073/pnas.1310493110.
[58] J. Sarin, M. Vuorenmaa, P.K. Vallittukka, R. Grénman, P. Boström, P. Riihilä, L. Nissinen, V.-M. Kähäri, J. Pulkkinen, The viability and growth of HaCaT cells after exposure to bioactive class S53P4-containing cell culture media, Otol. Neurotol. 42 (2021) e559, https://doi.org/10.1097/MAO.0000000000003057.–e567.
[59] M. Schürmann, P. Goon, H. Sudhof1, Review of potential medical treatments for middle ear cholesteatoma, Cell Commun. Signal. 20 (2022) 1–23, https://doi.org/10.1186/s12964-022-00953-w.
[60] S. Wilkesmann, J. Fellenberg, Q. Nawaz, B. Reible, A. Moghaddam, A. R. Boccaccini, F. Westhauser, Primary osteoblasts, osteoblast precursor cells or osteoblast-like cell lines: which human cell types are (most) suitable for characterizing 45S5-bioactive glass? J. Biomed. Mater. Res. 108 (2020) 663–674, https://doi.org/10.1002/jbm.a.36846.
[61] F. Kermani, A. Gharavian, S. Mollazadeh, S. Kargozar, A. Youssefi, J.V. Khaki, Silicon-doped calcium phosphates; the critical effect of synthesis routes on the biological performance, Mater. Sci. Eng. C 111 (2020), 110828, https://doi.org/10.1016/j.msec.2020.110828.
[62] W. Götz, E. Tobiasch, S. Witzleben, M. Schulze, Effects of silicon compounds on biomineralization, osteogenesis, and hard tissue formation, Pharmaceutics 11 (2019) 1–27, https://doi.org/10.3390/pharmaceutics11030117.
[63] C. Fan, Q. Xu, R. Hao, C. Wang, Y. Que, Y. Chen, C. Yang, J. Chang, Multi-functional wound dressings based on silicate bioactive materials, Biomaterials 287 (2022) 1–15, https://doi.org/10.1016/j.biomaterials.2022.121652.